Low albite: an X-ray and neutron diffraction study

GEORGE E. HARLOW

Department of Mineral Sciences
American Museum of Natural History
New York, New York 10024

AND GORDON E. BROWN, JR.

Department of Geology, Stanford University
Stanford, California 94305

Abstract

Least-squares refinements of the structure of low albite from Amelia, Virginia with three-dimensional neutron and X-ray diffraction intensity data sets yield weighted R factors of 0.024 and 0.035, respectively, with anisotropic thermal models. The two methods result in essentially identical positional parameters, though slight differences in thermal parameters may be due to the variation in relative scattering powers. Direct refinement of Al/Si occupancy of tetrahedral sites was possible for the neutron data but not for the X-ray data, resulting in the following values of $\langle \overline{T-O} \rangle$ (in Å) and Al occupancy (associated errors in parentheses): T_1O 1.743(1)Å, 0.97(2) Al; T_1m 1.609(1)Å, 0.04(2) Al; T_2O 1.614(1)Å, 0.0 Al; T_2m 1.616(1)Å, 0.0 Al. The difference between the refined T_1O occupancy and an Al-filled T_1O site is significant at a 90% confidence. When these data are combined with other neutron diffraction estimates of order/disorder for a low sanidine and Himalaya orthoclase, a non-linear plot of $\langle \overline{T-O} \rangle$ *vs.* Al content results, which is best fit with a 3rd-order polynomial. This curve differs from the linear plot by as much as 0.016Å in the high-Al region. However, direct comparison of average T–O bond lengths between ordered and disordered tetrahedra includes an apparent shortening in disordered feldspars (comparable to a thermal motion effect) which may amount to 0.003Å. Analysis of the apparent-thermal-motion anisotropy of the Na site with displacive split-site models yields a splitting distance of 0.39Å for both data sets, but a single-Na, anisotropic thermal model is preferred.

Introduction

Since Barth (1934) first suggested that the polymorphism of K-feldspars resulted from order–disorder of Al and Si atoms, a considerable effort has been made by crystallographers, mineralogists, and petrologists to characterize Al–Si distributions in natural and synthetic feldspars. The primary reasons for the intense interest in this subject are (1) the natural abundance of alkali feldspars in the Earth's crust and (2) their potential for geothermometry from a detailed knowledge of the composition-, temperature-, and pressure-dependence of intracrystalline Al–Si distributions. Smith's (1954) important synthesis of available structural data for feldspars provided the basis for all subsequent optical and cell-parameter methods for determining the degree of ordering of Al

and Si among the tetrahedral sites. He used the simple idea that Al-containing tetrahedra are larger than Si-containing ones and correlated mean T–O distances (T = Si,Al) with Al content of a tetrahedron. Later revision of Smith's study (Smith and Bailey, 1963) and statistical analyses of the correlation between mean T–O distance and % Al (Jones, 1968; Ribbe and Gibbs, 1969) have provided linear regression equations for this correlation. However, serious doubts about the linear relationship between mean T–O distance and Al content of tetrahedra were raised by Brown *et al.* (1969) and Ribbe *et al.* (1974), who pointed out a number of other factors which affect individual T–O distances in framework aluminosilicates. Because of these findings, the currently-used feldspar structural-state indicators, such as the lat-

tice-parameter method of Stewart and Wright (1974) for alkali feldspars, are in need of revision when enough new data become available. Ribbe (1975) has since proposed a method for estimating approximate Al contents of K-rich feldspars based on individual bond-length differences and which, according to Ribbe, eliminates concern about whether the correct Al content *vs.* T–O distance relationship is linear or nonlinear. This problem could be eliminated entirely if future structural-state determinations were based on direct measurements of Al–Si site distributions. However, such determinations have proven possible only by neutron diffraction experiments (see Prince *et al.*, 1973; Brown *et al.,* 1974), which are not feasible for more than a few samples.

Our study of the structure of a low albite with both X-ray and neutron-diffraction methods has been undertaken to help elucidate the relationship between Al–Si occupancy and T–O bond distances for this important end-member feldspar composition. In addition, we have examined general structural features, in particular the nature of apparent thermal motion of the Na atom, and have compared results from our independent X-ray and neutron structure refinements.

Table 1. Composition and cell constants of Amelia low albite

Composition:	wt.%[1]	cat./8 ox	wt.%[2]	cat./8 ox
SiO_2	69.4	3.024	68.06	2.976
Al_2O_3	19.0	0.976	20.00	1.031
Fe_2O_3	0.0	0.0	0.04	0.001
CaO	0.02	0.001	0.15	0.007
Na_2O	11.5	0.969	11.49	0.974
K_2O	0.10	0.006	0.15	0.009
	100.0	4.976	99.89	4.998
Ab	99.3		98.5	
Or	0.6		0.7	
An	0.1		0.8	

Cell Constants:

a	8.142(2) Å	α	94.19(2) deg.	
b	12.785(2)	β	116.61(2)	
c	7.159(2)	γ	87.68(2)	
V	664.5(9) Å^3			

[1] microprobe analysis

[2] analysis of Morey and Fournier (1961)

Experimental technique

Samples

Samples of low albite from Amelia County, Virginia were obtained from the late D. R. Waldbaum (for sample description see Waldbaum and Robie, 1971, sample no. 6306). For the neutron work a clear glassy rhomb of cleavelandite habit with a volume of 15.4 mm^3 was selected from a larger piece; an alternate crystal was chosen from a fragment cleaved from the same large piece. The X-ray sample, cleaved from the alternate neutron crystal, had a volume of 2.04×10^{-3} mm^3 with largest edge dimension of 0.4 mm. Sample composition from wet-chemical analysis and a microprobe analysis are listed in Table 1. Cell parameters were calculated with Burnham's LCLSQ IV least-squares program using X-ray powder data collected with a powder diffractometer on material identical to that examined in this experiment (see Table 1).

Neutron experiment

Neutron diffraction data for a half sphere of reciprocal space with $0.15 \leq \sin\theta/\lambda \leq 0.69$ were collected at the Brookhaven National Laboratories Hi Flux Beam Reactor on an automated (Brookhaven Multispectrometer Control System) four-circle diffractometer. The θ–2θ step incremental scan technique with a BF$_3$ proportional counter was used. The reactor had a thermal neutron flux of 7×10^{14} neutron/cm^2 sec at the end of the beam tube and a flux of $\sim 10^7$ neutron/cm^2 sec at the crystal (the low energy flux relative to that used in X-ray diffraction necessitates the large crystal size). A total of 1781 reflections was measured and after correction for background (by the method of Lehmann *et al.*, 1972), absorption, and dispersion (the last two both nil), averaging of equivalent reflections, and examination of peak shapes, 1633 reflections were selected for the initial least-squares refinement. The initial refinement was performed with a modified version of ORFLS on the BNL computer system with constant scattering factors: Na, 0.362; K, 0.370; Ca, 0.466; Si, 0.415 Al, 0.345; O, 0.5803; all $\times 10^{-12}$ cm/atom. Further refinements examining tetrahedral site occupancies and the alkali site were performed on the Princeton IBM 360/91 computer system using L. W. Finger's RFINE and RFINE II.

X-ray experiment

X-ray diffraction data for a half sphere of reciprocal space with $0.05 \leq \sin\theta/\lambda \leq 0.76$ were collected on

an automated Picker FACS-1 four-circle single-crystal diffractometer with Mo$K\alpha$ radiation (Zr filter). Data were collected using θ–2θ scan with a scan speed of 1° 2θ per minute, a 2° base width compensated for dispersion; background was measured at high and low 2θ limits for a total of 20 seconds. The initial data were corrected for background, set to a uniform level relative to standard reflection intensities (2 measured every 20 reflections), corrected for Lorentz polarization and absorption, and their extinction β's calculated by a modified version of C. T. Prewitt's ACACA that employed the Gaussian quadrature technique ($4 \times 4 \times 4$ grid) for absorption. A total of 2603 reflections were used for least-squares refinement, of which 2441 were not rejected on the criterion of the counting statistics standard deviation being less than F_{obs}. RFINE II was used for the least-squares refinements, refining on a single scale factor, isotropic extinction parameter (Zachariasen, 1967), positional parameters, and first isotropic and then anisotropic thermal parameters.

The neutron refinements, which preceded the X-ray ones, yielded a weighted R factor (R_w) and unweighted R factor (R_u) of 0.076 and 0.069 for the isotropic case and 0.024 and 0.021 for the anisotropic case (standard deviation of a unit weight observation = 1.29). We assumed fully ordered tetrahedral sites (T_1O occupied by Al, the excess in T_1m); initial parameters were those of low albite from Ribbe *et al.* (1969). Positional parameters (Table 3), tetrahedral bond lengths (Table 6), and O–T–O and T–O–T angles (Table 7) were taken from the anisotropic case; anisotropic β's, isotropic B's, and R.M.S. equivalent amplitudes are listed in Tables 4 and 5. At this stage, refinements on Al/Si occupancy of the four tetrahedral sites were performed using various chemically constrained and unconstrained models. The results are noted in Table 2 with the weighted R factors for each case.

The least-squares refinement of the X-ray data yielded isotropic R factors of 0.053 R_w and 0.071 R_u and anisotropic R factors of 0.035 R_w and 0.040 R_u (standard deviation of a unit weight observation = 5.36), with relativistic Dirac–Slater atomic scattering factors calculated by Cromer and Waber (1965) for neutral atoms and Al/Si ordering as determined in the neutron refinements. Similar results were obtained on fully ionized atoms (except oxygen—O^{-1}) with scattering factors calculated by Cromer and Mann (1968); differences are noted in the text. The scattering factor for the alkali site was a compositionally weighted average of the scattering factors for Na,

Table 2. Results for T-site occupancy refinements including significance levels

Model	Variables	Refinement Type	Al in T Sites				Rw
1	119	Occupancy I (chemistry constrained)	0.970 .019	0.035	0.0	0.0	0.021367
2	122	Occupancy II (unconstrained)	0.970 .027	0.035 .028	-0.003 .028	-0.022 .061	0.021342
3	121	Occupancy III (chemistry constrained)	0.975 .023	0.039 .023	0.021 .023	-0.017	0.0213465
4*	120	Occupancy IV (chemistry constrained)	0.973 .03	0.009 .04	0.0	0.0	0.021389
5	118	Constrained I (fully ordered)	1.00	0.05	0.0	0.0	0.021384
6	118	Constrained II (95% Al in T_{10})	0.95	0.10	0.0	0.0	0.021373
7	118	Constrained III (90% Al in T_{10})	0.90	0.15	0.0	0.0	0.021461
8	118	Constrained IV (80% Al in T_{10})	0.80	0.25	0.0	0.0	0.021928

R Factor Significance Tests

$R_{i,j} = R_{wi}/R_{wj}$

$R_{5,1} = 1.000810$

$R_{6,1} = 1.000287$

$R_{7,1} = 1.004393$

$R_{8,1} = 1.026279$

$R_{1,3} = 1.00095$

$R'_{b,n-m,\alpha} = [\frac{b}{n-m} \cdot F_{b,n-m,\alpha} + 1]^{\frac{1}{2}}$

$R_{1,1504,0.005} = 1.00271$

$R_{1,1504,0.010} = 1.0022$

$R_{1,1504,0.10} = 1.00088$

$R_{1,1504,0.25} = 1.00048$

$R_{1,1504,0.50} = 1.00016$

$R_{2,1501,0.75} = 1.00095$

* Not totally converged

Ca, and K. Positional parameters (Table 3), tetrahedral bond lengths (Table 6), and temperature factors (Tables 4 and 5) are listed with the values from the neutron refinements. An attempt to refine Al/Si occupancies of the tetrahedral sites resulted in unrealistic total site occupancies for neutral atoms and realistic occupancies but excessively large errors for ionized atoms. Consequently only T occupancies as determined by the neutron refinements are listed for the X-ray refinement results.

Two models employing split isotropic Na sites were refined for each data set; one uses two half atoms and the other uses two partial atoms, with one's occupancy refined and the other's occupancy constrained so that the total occupancy of both sites is equal to 1.0. The results are listed in Tables 3 and 8.

Results and discussion

General comparison of neutron and X-ray refinements

The two independently-derived sets of structural parameters (positions and apparent thermal motions)

Table 3. Atomic positional coordinates

Site		Occupancy	Spec.	X	Y	Z
T_1O	neutron	0.030(20)	Si	0.00901(10)	0.16862(6)	0.20806(11)
	x-ray	0.030	Si	0.00878(11)	0.16864(6)	0.20805(13)
T_1m	neutron	0.965	Si	0.00386(8)	0.82062(5)	0.23728(9)
	x-ray	0.965	Si	0.00382(10)	0.82064(5)	0.23734(11)
T_2O	neutron	1.0	Si	0.69209(8)	0.11036(5)	0.31508(9)
	x-ray	1.0	Si	0.69210(10)	0.11040(5)	0.31507(12)
T_2m	neutron	1.0	Si	0.68152(8)	0.88195(5)	0.36078(9)
	x-ray	1.0	Si	0.68175(10)	0.88189(5)	0.36071(12)
Na	neutron	0.986	Na	0.26849(13)	0.98870(10)	0.14672(18)
	x-ray			0.26839(18)	0.98867(12)	0.14628(24)
Na_1	neutron	0.526(17)	"Na"	0.27098(28)	0.97765(36)	0.16218(55)
	x-ray	0.533(26)	"Na"	0.27033(45)	0.97800(57)	0.16219(92)
Na_2	neutron	0.474	"Na"	0.26561(32)	0.00168(41)	0.12859(62)
	x-ray	0.467	"Na"	0.26617(45)	0.00103(64)	0.12793(101)
O_{A1}	neutron	1.0	O	0.00490(7)	0.12115(4)	0.96638(7)
	x-ray	1.0	O	0.00481(27)	0.12120(14)	0.96610(30)
O_{A2}	neutron	1.0	O	0.59229(6)	9.99755(4)	0.28053(7)
	x-ray	1.0	O	0.59166(24)	0.99766(14)	0.27967(30)
O_BO	neutron	1.0	O	0.81231(7)	0.11013(4)	0.19056(8)
	x-ray	1.0	O	0.81285(26)	0.11039(15)	0.19124(32)
O_Bm	neutron	1.0	O	0.82027(7)	0.85114(4)	0.25876(9)
	x-ray	1.0	O	0.82061(27)	0.85121(15)	0.25942(34)
O_CO	neutron	1.0	O	0.01342(6)	0.30252(4)	0.27026(8)
	x-ray	1.0	O	0.01348(25)	0.30276(14)	0.27023(31)
O_Cm	neutron	1.0	O	0.02398(7)	0.69389(4)	0.22991(8)
	x-ray	1.0	O	0.02402(26)	0.69390(14)	0.22938(32)
O_DO	neutron	1.0	O	0.20770(7)	0.10901(4)	0.38910(7)
	x-ray	1.0	O	0.20765(26)	0.10922(15)	0.38898(30)
O_Dm	neutron	1.0	O	0.18364(7)	0.86819(4)	0.43609(8)
	x-ray	1.0	O	0.18316(27)	0.86825(15)	0.43555(31)

Estimated standard errors in parentheses refer to the last digits.

have been compared for consistency of error by the method of half-normal probability plot analysis (Abrahams and Keve, 1971). Figure 1 shows two plots of ranked observed-parameter deviates Δ_i *vs.* ranked normal deviates X_i for all parameters and positional parameters only, as determined from equations and tables in Section 4.3 of Volume IV of *International Tables for X-ray Crystallography* (1974). The treatment and results are similar to those of Higgins and Ribbe (1979) for sapphirine. A scatter of points about a line of unit slope would indicate a correct estimate of error with no obvious contributions due to systematic error. The observed scatter approaching a line with a slope of two for all parameters suggests that there is little distinguishable systematic error but an underestimation of pooled standard deviations by a factor of about two. In the positional parameters alone there is more scatter, which either is insignificant and only a function of the small number of points (39), or is an indication of compounded real and systematic errors of roughly the same magnitude (Abrahams and Keve, 1971). The slope of the trend

for positional parameters is about 1.2, which suggests a realistic estimation of standard deviations. Hence, as might be expected, the estimation of error is more subject to bias and misevaluation for the anisotropic temperature factors than for positional parameters alone.

For the most part the refinements of the two data sets are identical within 1 or 2 standard errors of all parameters for the X-ray results. As indicated above, the largest variations occur for the thermal parameters. The neutron data, compared to the X-ray data, yield larger values of equivalent isotropic temperature factor (B) and anisotropic factor β_{33} for T and Na sites and yield smaller root-mean-squared (R.M.S.) displacements for oxygen sites. This is likely due in large part to the difference in relative scattering powers of Si, Al, Na, and O between X-ray and neutron diffraction. While it is tempting to use differences in the nature of the diffraction interaction between neutrons and X-rays to examine the asymmetry of bonding-electron distributions relative to nuclei, the variations in positional parameters and bond lengths and the evaluation of pooled errors suggest there are no measurable asymmetries.

Table 4. Thermal parameters

Site		Equivalent B	R.M.S. Amplitudes in Å		
			Axis 1	Axis 2	Axis 3
T_1O	neutron	0.599(11)	0.0759(20)	0.0851(18)	0.0988(17)
	x-ray	0.436(12)	0.0728(25)	0.0747(23)	0.0972(19)
T_1m	neutron	0.512(9)	0.0711(17)	0.0803(15)	0.0891(15)
	x-ray	0.436(12)	0.0759(24)	0.0659(25)	0.0892(18)
T_2O	neutron	0.532(9)	0.0768(15)	0.0792(15)	0.0898(15)
	x-ray	0.464(12)	0.0615(24)	0.0772(21)	0.0889(19)
T_2m	neutron	0.532(9)	0.0768(15)	0.0792(16)	0.0898(15)
	x-ray	0.462(12)	0.0623(24)	0.0808(21)	0.0845(20)
Na	neutron	2.663(20)	0.1221(16)	0.1311(15)	0.2628(15)
	x-ray	2.529(29)	0.1169(28)	0.1306(25)	0.2557(22)
O_{A1}	neutron	0.946(7)	0.0739(13)	0.1149(9)	0.1314(8)
	x-ray	0.917(30)	0.0733(58)	0.0987(43)	0.1404(35)
O_{A2}	neutron	0.720(7)	0.0775(12)	0.0915(10)	0.1139(9)
	x-ray	0.754(28)	0.0748(52)	0.0936(44)	0.1196(39)
O_BO	neutron	1.040(8)	0.0791(13)	0.1162(10)	0.1405(8)
	x-ray	1.030(31)	0.0930(48)	0.1086(44)	0.1367(37)
O_Bm	neutron	1.319(8)	0.0787(13)	0.1410(9)	0.1551(8)
	x-ray	1.258(33)	0.0862(51)	0.1323(38)	0.1512(37)
O_CO	neutron	0.918(8)	0.0805(12)	0.1102(10)	0.1276(9)
	x-ray	0.945(31)	0.0800(50)	0.1165(41)	0.1262(40)
O_Cm	neutron	0.935(8)	0.0823(12)	0.1087(10)	0.1302(9)
	x-ray	0.981(31)	0.0776(52)	0.1083(42)	0.1397(37)
O_DO	neutron	1.020(8)	0.0868(12)	0.1180(9)	0.1316(9)
	x-ray	1.051(31)	0.0824(54)	0.1091(42)	0.1458(36)
O_Dm	neutron	1.153(8)	0.0868(12)	0.1180(9)	0.1316(9)
	x-ray	1.190(33)	0.0842(53)	0.1152(41)	0.1517(36)

Estimated standard errors in parentheses refer to the last digits.

Refinement of Al/Si order

As there is a uniform 18.5% difference in the scattering power of Al and Si in neutron diffraction (compared with an average 9% for X-rays) a meaningful refinement of the occupancy of the four T sites in low albite was possible. Many models involving either unconstrained or constrained occupancy of the T sites were refined (see Table 2). Those models involving variation of T_2O and T_2m occupancies led to results requiring Si occupancies either in excess of or insignificantly different from 1.0, as in model 2. Consequently final tetrahedral occupancy refinements involved variation in the T_1 sites only. However, it is encouraging to note that cases like model 2 are essentially identical to model 1 when errors are considered.

The *R*-factor ratio test of Hamilton (1965) was used to examine the constrained and unconstrained models of T_1O and T_1m occupancy; the results are shown in Table 2. The unconstrained case (model 1) is shown to be superior at better than the 75% significance level for all but model 6, which is within the standard error of the refined occupancy. In Figure 2, a diagrammatic curve has been drawn with the standard error in occupancy and the *R*-test significance levels marked along the ordinate and the Al content of the T_1O site along the abscissa, to show the nature of the data refinements upon tetrahedral occu-

Table 5. Root-Mean-Square amplitudes of apparent thermal vibration

Site		B	β_{11}	β_{22}	β_{33}	β_{12}	β_{13}	β_{23}
					$\beta \times 10^5$			
T_1O	n	0.597(36)	326(12)	98(4)	314(15)	-29(5)	163(11)	10(6)
	x	0.555(19)	333(14)	70(4)	263(17)	-20(6)	128(13)	2(7)
T_1m	n	0.601(31)	266(9)	87(3)	278(12)	15(4)	147(9)	14(5)
	x	0.450(17)	277(12)	56(4)	219(15)	21(5)	114(11)	13(6)
T_2O	n	0.607(31)	259(10)	73(3)	381(13)	-12(4)	143(9)	19(5)
	x	0.473(17)	246(12)	46(4)	306(15)	-2(5)	90(11)	0(6)
T_2m	n	0.636(31)	228(9)	79(3)	380(13)	5(4)	138(9)	25(5)
	x	0.464(17)	250(12)	49(4)	318(16)	11(5)	116(11)	15(6)
Na	n	2.510(59)	580(15)	591(8)	1548(25)	-100(9)	400(15)	-515(1)
	x	1.972(40)	620(24)	524(11)	1468(40)	-80(12)	356(25)	-516(1)
Na_1	n	1.356(64)						
	x	1.374(81)						
Na_2	n	1.413(71)						
	x	1.285(94)						
O_{A1}	n	0.979(27)	641(8)	159(3)	368(10)	-11(4)	304(7)	37(4)
	x	0.974(4)	716(36)	121(11)	333(42)	27(15)	296(33)	23(17)
O_{A2}	n	0.758(26)	311(7)	78(2)	581(10)	-5(3)	165(7)	43(4)
	x	0.763(4)	336(30)	69(9)	585(44)	-4(13)	127(31)	28(16)
O_BO	n	1.098(27)	461(8)	174(3)	805(11)	-92(4)	419(8)	-29(4)
	x	1.083(5)	518(34)	146(11)	788(49)	-67(15)	406(35)	-31(1)
O_Bm	n	1.330(28)	542(8)	233(3)	1076(12)	89(4)	582(8)	40(5)
	x	1.267(5)	593(36)	174(11)	1051(55)	97(16)	531(38)	28(20)
O_CO	n	0.971(27)	404(8)	98(2)	754(11)	-57(3)	237(8)	-20(4)
	x	0.984(4)	523(34)	82(10)	661(47)	-25(15)	217(34)	-27(17)
O_Cm	n	0.995(26)	421(8)	92(2)	701(10)	39(3)	167(7)	33(4)
	x	0.970(4)	485(33)	82(10)	672(47)	48(14)	128(33)	14(17)
O_DO	n	1.040(27)	476(8)	175(3)	409(10)	39(4)	84(7)	44(4)
	x	1.072(5)	564(35)	145(11)	403(45)	66(15)	55(33)	47(18)
O_Dm	n	1.177(27)	542(8)	180(3)	431(10)	-55(4)	12(7)	-15(4)
	x	1.213(5)	634(36)	152(11)	436(46)	-40(16)	-2(34)	-26(18)

Estimated standard errors in parentheses refer to the last digits.
* n - neutron; x - X-ray

Table 6. T–O and tetrahedral O–O bond distances

$T_1$0- O	neutron	x-ray	T_1m- 0	neutron	x-ray
O_{A1}	1.7472(9)	1.749(2)	O_{A1}	1.5955(8)	1.594(2)
O_BO	1.7446(10)	1.739(2)	O_Bm	1.6000(9)	1.599(2)
O_CO	1.7348(9)	1.737(2)	O_Cm	1.6214(8)	1.621(2)
O_DO	1.7448(10)	1.744(2)	O_Dm	1.6179(8)	1.614(2)
Average	1.7429	1.742	Average	1.6087	1.607

$T_2$0- O	neutron	x-ray	T_2m- O	neutron	x-ray
O_{A2}	1.6322(8)	1.633(2)	O_{A2}	1.6448(8)	1.650(2)
O_BO	1.5918(8)	1.592(2)	O_Bm	1.6205(8)	1.617(2)
O_Cm	1.6171(8)	1.617(2)	O_CO	1.5957(8)	1.594(2)
O_DO	1.6152(8)	1.619(2)	O_DO	1.6015(8)	1.603(2)
Average	1.6141	1.615	Average	1.6156	1.616

$T_1$0	neutron	x-ray	T_1m	neutron	x-ray
O_{A1}- O_BO	2.7310(9)	2.732(3)	O_{A1}- O_Bm	2.6010(9)	2.610(3)
- O_CO	2.9528(10)	2.955(3)	- O_Cm	2.6747(8)	2.671(3)
- O_DO	2.7525(8)	2.753(3)	- O_Dm	2.5883(8)	2.583(3)
O_BO- O_CO	2.881(8)	2.886(3)	O_Bm- O_Cm	2.6100(8)	2.612(3)
- O_DO	2.8783(10)	2.874(3)	- O_Dm	2.6570(10)	2.651(3)
O_CO- O_DO	2.8518(8)	2.852(3)	O_Cm- O_Dm	2.6210(8)	2.620(3)
Average	2.8424	2.842	Average	2.6253	2.625

$T_2$0	neutron	x-ray	T_2m	neutron	x-ray
O_{A2}- O_BO	2.6595(9)	2.662(3)	O_{A2}- O_Bm	2.6258(8)	2.631(3)
- O_Cm	2.5653(7)	2.563(3)	- O_CO	2.5875(7)	2.585(2)
- O_DO	2.6115(8)	2.618(3)	- O_DO	2.6349(8)	2.543(3)
O_BO- O_Cm	2.6612(9)	2.660(3)	O_Bm- O_CO	2.6367(10)	2.636(3)
- O_DO	2.6524(8)	2.652(3)	- O_DO	2.6428(8)	2.640(3)
O_Cm- O_DO	2.6533(9)	2.659(3)	O_CO- O_DO	2.6884(9)	2.687(3)
Average	2.6339	2.636	Average	2.6365	2.637

Estimated standard errors in parentheses refer to the last digits.

pancies. The results indicate that there is not much difference between completely-ordered low albite and the partially-disordered one achieved by refinement with chemical constraints, but that in any case there is a high degree of ordering.

T–O bond distances and Al/Si ordering

With the completion of these refinements, four more points are available for determination and refinement of the relationship between tetrahedral bond distance and Al/Si occupancy in the alkali feldspars. With values determined in other neutron diffraction experiments for a Himalaya orthoclase (Prince *et al.*, 1973) and a low sanidine (Brown *et al.*, 1974) (see Table 8), least-squares refinements of the data to fit polynomial curves of the form

$$Al/(Al + Si) = \sum_{i=0}^{n} \langle \overline{T-O} \rangle^i$$

Table 7. O–T–O and T–O–T angles

O –T$_1$O–O		neutron	x-ray	O –T$_1$m–O		neutron	x-ray
O$_{A1}$–	–O$_B$O	102.91(5)	103.1(1)	O$_{A1}$–	–O$_B$m	109.50(5)	109.6(1)
	–O$_C$O	115.99(5)	115.9(1)		–O$_C$m	112.50(5)	112.3(1)
	–O$_D$O	104.04(5)	104.0(1)		–O$_D$m	108.23(5)	108.4(1)
O$_B$O–	–O$_C$O	112.21(5)	112.3(1)	O$_B$m–	–O$_C$m	108.23(5)	108.4(1)
	–O$_D$O	111.16(5)	111.2(1)		–O$_D$m	111.31(5)	111.2(1)
O$_C$O–	–O$_D$O	110.08(5)	110.0(1)	O$_C$m–	–O$_D$m	108.02(5)	108.2(1)
Average		109.40	109.4	Average		109.48	109.5

O –T$_2$O–O		neutron	x-ray	O –T$_2$m–O		neutron	x-ray
O$_{A2}$–	–O$_B$O	111.15(5)	111.3(1)	O$_{A2}$–	–O$_B$m	107.21(4)	107.3(1)
	–O$_C$m	104.23(4)	104.1(1)		–O$_C$O	105.96(4)	105.7(1)
	–O$_D$m	107.06(4)	107.2(1)		–O$_D$O	108.51(4)	108.7(1)
O$_B$O–	–O$_C$m	112.06(5)	112.0(1)	O$_B$m–	–O$_C$O	110.14(5)	110.3(1)
	–O$_D$m	111.60(5)	111.4(1)		–O$_D$O	110.22(5)	110.2(1)
O$_C$m–	–O$_D$m	110.34(5)	110.6(1)	O$_C$O–	–O$_D$O	114.46(5)	114.4(1)
Average		109.42	109.4	Average		109.42	109.4

	neutron	x-ray
T$_1$O–O$_{A1}$–T$_1$m	141.45(5)	141.5(1)
T$_2$m–O$_{A2}$–T$_2$θ	130.08(4)	129.7(1)
T$_1$O–O$_B$O–T$_2$O	139.66(5)	129.8(1)
T$_1$m–O$_B$m–T$_2$m	161.20(5)	161.5(2)
T$_1$O–O$_C$O–T$_2$m	129.88(5)	129.8(1)
T$_1$m–O$_C$m–T$_2$O	135.85(5)	135.8(1)
T$_1$O–O$_D$O–T$_2$m	133.95(5)	133.9(1)
T$_1$m–O$_D$m–T$_2$O	151.84(5)	151.8(2)
Average	140.49	140.5

Estimated standard errors in parentheses refer to the last digits.

were performed, where Al/(Al + Si) is the fraction of Al in a site and $\langle\overline{\text{T–O}}\rangle$ is the average inter-atomic distance between the T site and its surrounding four oxygens. Though there was little difference between the fully-ordered and partially-disordered low-albite models refined, both were used in polynomial curve fitting. Results are shown in Table 9 and Figure 3.

To test for the best fit, three criteria were used. First, is the fit physically realistic? Fits with significant negative curvatures or fits that require excess Al or Si beyond known limits were considered unrealistic and, hence, were discarded. Second, the standard error of any of the polynomial coefficients must be less than that coefficient itself. Third, a variance ratio test (Hamilton, 1964) was used to discriminate among polynomials of successive degrees. Consequently, polynomials of degree three are preferred, but the curve for the constrained model is more realistic as it does reach full Al occupancy [Al/(Al + Si)

= 1.0]. The results show that there can be a large discrepancy in predicted bond lengths between linear and non-linear models; there is a difference of 0.016Å at Al/(Al + Si) ≃ 0.9. The net effect is an increase in the apparent amount of Al in a T site with $\langle\overline{\text{T–O}}\rangle$ lengths between 1.65 and 1.74Å for the non-linear model. However, these curves should not be considered determinative and, hence, have not been plotted. $\langle\text{T–O}\rangle$ and refined occupancy data for alkali feldspars with a structural state between that of orthoclase and low albite are needed before determinative plots may be usable. Even then, other factors (Ribbe *et al.*, 1974) must be considered. Presently, the indication is that such plots may not be linear.

One important point that has been overlooked is the effect of disorder on T–O distances. Examination of the refinements of a number of feldspar structures shows that disordered feldspars generally have shorter grand-mean-average T–O bond lengths than do ordered ones. In Table 9 the grand-mean-average of T–O bond lengths for ordered alkali feldspar structures are 0.001 to 0.003Å longer than for the disordered ones. A comparison has also been made for the $\langle\overline{\text{T–O}}\rangle$ values calculated from the Ribbe–Gibbs linear model and our 3rd-degree polynomial model; the differences in average bond lengths are less for the polynomial model but are still significant. The displacement of the individual Al and Si atoms from

Table 8. Polynomial regressions for neutron-determined feldspar occupancy data. Equations for the polynomial and the variance ratio test (V_R) are listed

$$\text{Al/(Al+Si)} = \sum_{i=0}^{n} a_i \langle\text{T–O}\rangle^i$$

A Partially Disordered (T$_1$O=0.970Al; T$_1$m=0.035)

	1st Order	2nd Order	3rd Order	4th Order
a_0	12.176±0.063	-45.493±130.0	4115.563±8.0x10^5	257089.983±5.2x10^4
a_1	7.559±0.023	47.393±186.0	-7432.206±2.6x10^6	-616138.021±1.8x10^5
a_2	-	-11.895± 16.6	4467.471±9.4 10^5	553563.260±1.6x10^5
a_3	-	-	-893.744±3.7x10^4	-220974.678±6.1x10^5
a_4				33069.047 1.3x10^4
$\Sigma\epsilon_i^2$	0.01197	0.00889	0.00379	0.00194
V_R	-	2.043	6.714	3.828

B Fully Ordered (T$_1$O=1.0Al; T$_1$m=0.05)

	1st Order	2nd Order	3rd Order
a_0	-12.619±0.203	-43.698± 8.60	3203.074± 625.0
a_1	7.828±0.124	44.986±10.30	-5791.239±1120.0
a_2	-	-11.095± 3.07	3484.116± 670.0
a_3			- 697.382± 134.0
$\Sigma\epsilon_i^2$	0.00786	0.00517	0.00192
V_R	-	3.127	8.486

$$V_R = (N-n)\frac{\Sigma\epsilon_i^2(n-1)-\Sigma\epsilon_i^2(n)}{\Sigma\epsilon_i^2(n)}$$

the averaged T sites yields an underestimate of the T–O distances relative to a simple average of the individual Si–O and Al–O bond lengths. The effect is much the same for evaluating the effect of thermal motion on bond lengths. Consequently, since disorder displacements are included in the thermal parameter, $\langle \overline{T-O} \rangle$ values should be corrected for some model of thermal motion, probably something between riding motion and noncorrelated motion (see Ohashi and Finger, 1974; Harlow, 1977). It would be better to use some common correction scheme for thermal (and disordering) effects in calculating a regression against Al/(Al + Si), but this is not possible for lack of such information on the other neutron refinements. However, it is likely that the points for disordered feldspars would be increased to higher $\langle \overline{T-O} \rangle$ values relative to those of low albite in Figure 3.

Na site—anisotropy vs. splitting

The Na site in both low and high albite displays a large apparent thermal motion anisotropy (*e.g.* Ferguson *et al.*, 1958; Williams and Megaw, 1964; Ribbe *et al.*, 1969; Quareni and Taylor, 1971). Ribbe *et al.* (1969) examined a model with two split isotropic atoms to approximate the anisotropy, in order to see
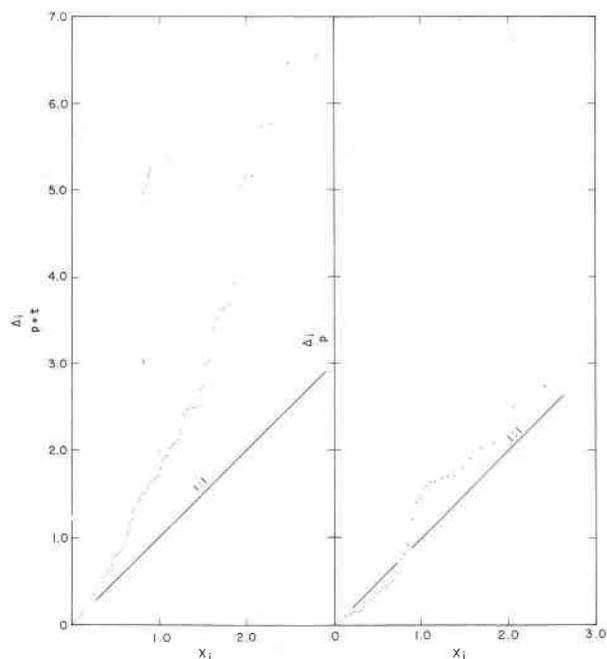
Fig. 2. Plot of R_{ij}, the R-factor ratio between the fixed T-site occupancy and refined occupancy models, and the amount of Al in the T_1O site. The significance levels and the standard error in refined T_1O occupancy are shown with dashed lines.

whether there might really be two loci for Na in the structure. Based on detailed calculations by Megaw in their paper, they could not distinguish between the time-average and the space-average models for their data, because there was inadequate separation between the split atoms. We have used a similar approach for our data, as earlier described. These results are listed in Table 10 along with the significance calculations for comparison of the various models.

Among the space-average models, the refined-occupancy model is preferred statistically for both neutron and X-ray data, though there are not large differences between the models. A direct comparison of R factors can be made between the anisotropic (time-average) model and the refined-occupancy split-atom (space-average) model, as they have the same number of refineable parameters. For both the neutron and X-ray data, the anisotropic model yields a smaller weighted R factor and hence appears to be a better model. In comparison with the Na-site modelling for low albite of Ribbe *et al.* (1969), the anisotropic models are very similar within the limits of error, though errors here are lower. Differences for the split-site modelling are greater, though not much more than 1 or 2 standard errors; in particular the $Na_1–Na_2$ splitting distances here are larger, 0.39 *vs.* 0.36Å for

Fig. 1. Half-normal probability plots comparing positional and thermal (left) and only positional (right) parameters between the X-ray and neutron refinements of low albite.

Table 9. Comparison of T–O bond distances between ordered and disordered alkali feldspars

	Total Al per Formula Unit	Or Content	$\overline{\langle\overline{T\text{-}O}\rangle}_O$*	$\overline{\langle\overline{T\text{-}O}\rangle}_{C1}$	Δ_1	$\overline{\langle\overline{T\text{-}O}\rangle}_{C2}$	Δ_2	
Ordered								
Low Microcline	1.00	99.	1.6442	1.6430	12	1.6443	– 1	Brown and Bailey (1964)
Low Microcline	1.00	100.	1.644	1.6430	10	1.6443	– 3	Finney and Bailey (1964)
Low Albite (X-ray)	1.001	0.6	1.6451	1.6430	21	1.6443	8	This study
Low Albite	1.00	0.	1.6444	1.6430	14	1.6443	1	Wainwright and Starkey (1968)
Microcline (CA1E)	1.015	88.6	1.6454	1.6436	18	1.6446	8	Dal Negro et al. (1978)
Microcline (RC20C)	1.012	88.5	1.6443	1.6434	9	1.6445	– 2	Dal Negro et al. (1978)
			Av. 1.6446		Av. 14		Av. 2	
Partially Disordered								
Orthoclase (neutron)	0.99	90.	1.6419	1.6430	–11	1.6443	–23	Prince et al. (1973)
Orthoclase	1.012	90.	1.6419	1.6434	–15	1.6446	–27	Colville and Ribbe (1968)
Adularia	1.00	88.1	1.6433	1.6430	3	1.6443	–10	Phillips and Ribbe (1973)
Adularia	1.001	88.	1.6427	1.6430	– 3	1.6443	–16	Harlow (unpublished)
Low Sanidine	1.00	85.	1.6431	1.6430	1	1.6443	–12	Phillips and Ribbe (1973)
Low Sanidine	1.00	85.	1.6408	1.6430	–22	1.6443	–35	Ohashi and Finger (1974)
Microcline (P1C)	1.012	90.0	1.6425	1.6434	– 9	1.6445	–20	Dal Negro et al. (1978)
Microcline (CA1B)	1.015	88.6	1.6438	1.6436	2	1.6446	– 8	Dal Negro et al. (1978)
Microcline (A1D)	1.011	90.4	1.6423	1.6434	–11	1.6445	–22	Dal Negro et al. (1978)
Microcline P17C)	1.001	87.1	1.6419	1.6430	–11	1.6443	–24	Dal Negro et al. (1978)
Microcline (CA1A)	1.015	88.6	1.6441	1.6436	5	1.6446	– 5	Dal Negro et al. (1978)
Microcline (P2A)	1.014	93.1	1.6443	1.6435	8	1.6446	– 3	Dal Negro et al. (1978)
Microcline	1.014	84.6	1.6428	1.6435	– 7	1.6446	–18	Bailey (1969)
Sanidine	1.018	87.	1.6438	1.6437	1	1.6447	– 9	Weitz (1972)
			Av. 1.6428		Av. – 5		Av. –16	
Disordered								
Sanidine (P2B)	1.014	93.1	1.6443	1.6435	8	1.6446	– 3	Dal Negro et al. (1978)
Heated Sanidine	1.018	87.	1.6428	1.6437	– 9	1.6447	–19	Weitz (1972)
High Sanidine								
(heated orthoclase)	1.025	92.	1.6421	1.6439	–18	1.6449	–28	Ribbe (1963)
High Albite	1.007	1.6	1.6434	1.64333	1	1.6444	–10	Ribbe et al. (1969)
High Albite	1.00	0.	1.6434	1.6430	4	1.6443	– 9	Wainright (see Smith, 1974)
Anorthoclase	1.008	32.5	1.6418	1.6433	–15	1.6445	–17	Harlow (in prep.)
Anorthoclase	1.069	22.3	1.6437	1.6456	–19	1.6460	–23	Harlow (in prep.)
Anorthoclase	1.025	13.8	1.6434	1.6439	– 5	1.6449	–15	Harlow (in prep.)
			Av. 1.6431		Av. – 7		Av. –17	

*O   Observed grand mean average

C_1 Calculated from total Al using $\langle\overline{T\text{-}O}\rangle = Al/(4 \times 6.58) + 1.605$ (Ribbe and Gibbs, 1969)

C_2 Calculated using 3rd order polynomial (fully ordered albite)
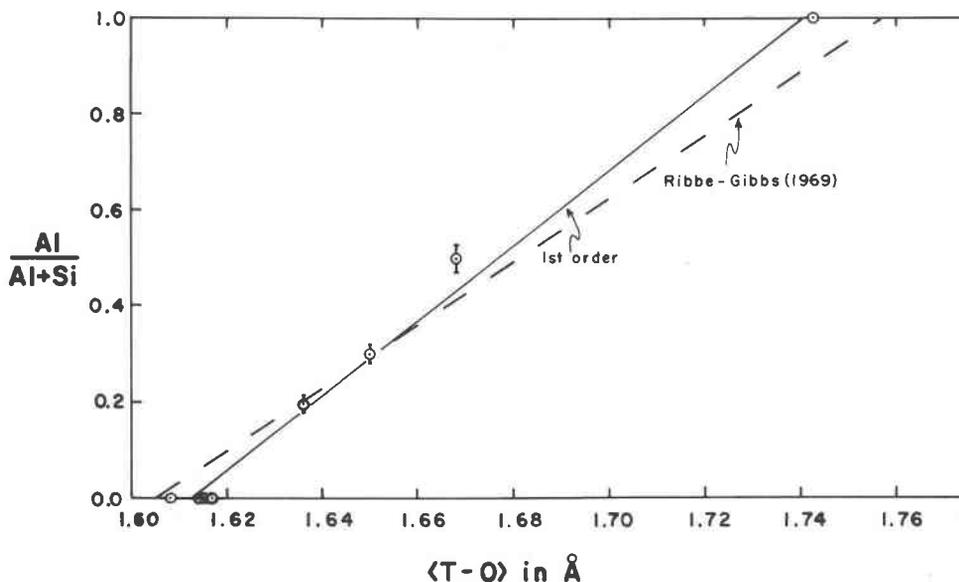
Fig. 3. Plot of average tetrahedral bond lengths for individual tetrahedra vs. occupancy, Al/(Al+Si), of the site as determined by direct refinement of neutron diffraction data. Points include low albite (constrained, full occupancy of T_1O), Himalaya orthoclase (Prince et al., 1973), and sanidine (Brown et al., 1974). A linear model for the data is shown.

Table 10. Results for anisotropic and split-site modelling of Na site including Na–O bond distances

Model		R_w	Occupancy Na$_1$	Splitting (Å)	Direction of Splitting* to a	to b	to c
1[†]	neutron	0.02138			101.0(8)	145.4(5)	51.9(5)
	x-ray	0.03541			103.5(13)	142.9(5)	49.1(5)
2	neutron	0.02237	0.5	0.392(3)	101.1	145.3	51.7
	x-ray	0.03599	0.5	0.387(4)	102.9	143.3	49.6
3	neutron	0.02235	0.526(17)	0.393(3)	101.2	145.3	51.7
	x-ray	0.03597	0.533(26)	0.393(3)	101.2	145.3	49.5

[†] 1-Anisotropic; 2-Split half atom; 3-split site, refine occupancy
*for the anisotropic case this refers to the direction of the major axis of the anisotropic ellipsoid

			Significance Level	
			(90%)	(75%)
		$R = R_{w2}/R_{w3}$	$R_{1,n,0.10}$	$R_{1,n,0.25}$
neutron	(n=1515)	1.00083	1.00087	1.00048
x-ray	(n=2322)	1.0004	1.0057	1.00031

Na – O Bond Distances (Å)

	Na(0000)		Na$_1$		Na$_2$	
	neutron	x-ray	neutron	x-ray	neutron	x-ray
O_{A1}(0000)	2.671(1)	2.671(2)	2.801(2)	2.797(4)	2.527(2)	2.535(4)
O_{A1}(000C)	2.537(1)	2.537(2)	2.458(2)	2.456(4)	2.644(2)	2.643(4)
O_{A2}(0000)	2.372(1)	2.369(2)	2.380(2)	2.381(4)	2.381(2)	2.372(4)
O_{A2}(000C)	3.724(1)	3.719(3)	3.837(3)	3.837(5)	3.600(3)	3.590(5)
O_{A2}(000C)	3.725(1)	3.733(3)	3.623(3)	3.627(5)	3.853(3)	3.863(5)
O_B(000C)	2.461(1)	2.464(2)	2.492(2)	2.499(4)	2.442(2)	2.438(4)
O_B(m00C)	3.465(2)	3.466(3)	3.640(3)	3.641(5)	3.261(3)	3.265(5)
O_C(0zi0)	2.961(L)	2.959(2)	2.835(2)	2.839(4)	3.116(2)	3.106(4)
O_C(mzi0)	3.266(1)	3.267(2)	3.390(3)	3.390(5)	3.127(3)	3.131(4)
O_D(0000)	2.437(1)	2.440(2)	2.451(2)	2.447(4)	2.438(2)	2.449(4)
O_D(m000)	2.996(2)	2.997(3)	2.835(3)	2.834(4)	3.188(3)	3.188(5)

Estimated errors in parentheses refer to last digits

the Ribbe *et al.* model. With Megaw's theoretical approach to distinguish the models, for our data the lower limit for splitting is 0.36Å for the neutron data and 0.33Å for the X-ray data; these limits are slightly smaller than those for the refined splittings. These results tend to support the time-average position model, though not with any great certainty. Using data collected at 300° and 600°C, Quareni and Taylor (1971) concluded that anisotropic thermal motion was the correct solution for Na in low albite. More recently Winter *et al.* (1977) examined the Na anisotropy of a Tiburon, California low albite at various elevated temperatures; they found that their measured apparent-thermal-motion magnitudes extrapolate to zero at 0K, which indicates that real thermal motion is the source of the large Na-site anisotropic delocalization. Since our results agree, we conclude that thermal motion is the most reasonable interpretation for the Na-site anisotropy.

Acknowledgments

References

Abrahams, S. C. and E. T. Keve (1971) Normal probability plot analysis of error in measured and derived quantities and standard deviations. *Acta Crystallogr., A27,* 157–165.

Bailey, S. W. (1969) Refinement of an intermediate microcline structure. *Am. Mineral., 54,* 1540–1545.

Barth, T. F. W. (1934) Polymorphic phenomena and crystal structure. *Am. J. Sci., 27,* 273–286.

Brown, B. E. and S. W. Bailey (1964) The structure of maximum microcline. *Acta Crystallogr., 17,* 1391–1400.

Brown, G. E., G. V. Gibbs and P. H. Ribbe (1969) The nature and variation in length of the Si–O and Al–O bonds in framework silicates. *Am. Mineral., 54,* 1044–1061.

———, W. C. Hamilton and C. T. Prewitt (1974) Neutron diffraction study of Al/Si ordering in sanidine: a comparison with X-ray diffraction data. In W. S. MacKenzie and J. Zussman, Eds., *The Feldspars,* p. 68–80. Manchester University Press, Manchester, England.

Colville, A. A. and P. H. Ribbe (1968) The crystal structure of an adularia and a refinement of the structure of orthoclase. *Am. Mineral., 53,* 25–27.

Cromer, D. T. and J. B. Mann (1968) X-ray scattering factors computed from numerical Hartree–Fock wave functions. *Acta Crystallogr., A24,* 321–324.

——— and J. T. Waber (1965) Scattering factors computed from relativistic Dirac–Slater wave functions. *Acta Crystallogr., 18,* 104–109.

Dal Negro, A., R. De Pieri, S. Quareni and W. H. Taylor (1978) The crystal structures of nine K feldspars from the Adamello massif (northern Italy). *Acta Crystallogr., B34,* 2699–2707.

Ferguson, R. B., R. J. Traill and W. H. Taylor (1958) The crystal structures of low-temperature and high-temperature albites. *Acta Crystallogr., 11,* 331–348.

Finney, J. J. and S. W. Bailey (1964) Crystal structure of an authigenic maximum microcline. *Z. Kristallogr., 119,* 413–436.

Hamilton, W. C. (1964) Section 4–6. Multivariate linear hypotheses. In W. C. Hamilton, Ed., *Statistics in Physical Science,* p. 139–142. Ronald Press Company, New York.

——— (1965) Significance tests on the crystallographic R factor. *Acta Crystallogr., 18,* 502–510.

Harlow, G. E. (1977) *The Anorthoclase Structures: a Room and High-temperature Study.* Ph.D. Dissertation, Princeton University, Princeton, New Jersey.

Higgins, J. B. and P. H. Ribbe (1979) Sapphirine II: A neutron and X-ray diffraction study of (Mg–Al)^{VI} and (Si–Al)^{IV} ordering in monoclinic sapphirine. *Contrib. Mineral. Petrol., 68,* 357–368.

International Tables for X-ray Crystallography, Vol. 4. (1974) Kynoch Press, Birmingham, England.

Jones, J. B. (1968) Al–O and Si–O tetrahedral distances in aluminosilicate framework structures. *Acta Crystallogr., B24,* 355–358.

Lehmann, M. S., W. C. Hamilton and F. K. Larsen (1972) Background determination for step-scan Bragg reflections. *Am. Crystallogr. Assoc. Meeting, Albuquerque, N.M.,* Abstract 09, 87.

Morey, G. W. and R. O. Fournier (1961) The decomposition of microcline, albite, and nepheline in hot water. *Am. Mineral., 96,* 688.

Ohashi, Y. and L. W. Finger (1974) Refinement of the crystal structure of sanidine at 25° and 400°. *Carnegie Inst. Wash. Year Book 73–74,* 539–544.

Phillips, M. W. and P. H. Ribbe (1973) The structures of monoclinic potassium-rich feldspars. *Am. Mineral., 58,* 495–499.

Prince, E., G. Donnay and R. F. Martin (1973) Neutron structure refinement of an ordered orthoclase. *Am. Mineral., 58,* 500–507.

Quareni, S. and W. H. Taylor (1971) Anisotropy of the sodium atom in low albite. *Acta Crystallogr., B27,* 281–285.

Ribbe, P. H. (1963) A refinement of the crystal structure of sanidinized orthoclase. *Acta Crystallogr., 16,* 426–427.

———— (1975) The chemistry, structure, and nomenclature of feldspars. In P. H. Ribbe, Ed., *Feldspar Mineralogy,* p. R1–R72. Mineral. Soc. Am. Short Course Notes, Vol. 2.

———— and G. V. Gibbs (1969) Statistical analysis of mean Al/Si–O bond distances and the aluminum content of tetrahedra in feldspars. *Am. Mineral., 54,* 85–94.

————, M. W. Phillips and G. V. Gibbs (1974) Tetrahedral bond length variations in feldspars. In W. S. MacKenzie and J. Zussman, Eds., *The Feldspars,* p. 25–48. Manchester University Press, Manchester, England.

————, H. D. Megaw, W. H. Taylor, R. B. Ferguson and R. J. Traill (1969) The albite structures. *Acta Crystallogr., B25,* 1503–1518.

Smith, J. V. (1954) A review of Al–O and Si–O distances. *Acta Crystallogr., 7,* 479–481.

———— and S. W. Bailey (1963) Second review of Al–O and Si–O tetrahedral distances. *Acta Crystallogr., 16,* 801–811.

Stewart, D. B. and T. L. Wright (1974) Al/Si order and symmetry of natural alkali feldspars, and the relationship of strained cell parameters to bulk composition. *Bull. Soc. fr. Minéral. Cristallogr., 97,* 356–377.

Waldbaum, D. R. and R. A. Robie (1971) Calorimetric investigation of Na–K mixing and polymorphism in the alkali feldspars. *Z. Kristallogr., 134,* 381–420.

Wainwright, J. E. and J. Starkey (1968) Crystal structure of a metamorphic low albite (abstr.). *Geol. Soc. Am. Abstracts with Programs,* 310.

Weitz, G. (1972) Die Struktur des Sanidins bei verschiedenen Ordnungs graden. *Z. Kristallogr., 136,* 418–426.

Williams, P. P. and H. D. Megaw (1964) The crystal structures of high and low albites at −180°C. *Acta Crystallogr., 17,* 882–890.

Winter, J. K., S. Ghose and F. P. Okamura (1977) A high-temperature study of the thermal expansion and the anisotropy of the sodium atom in low albite. *Am. Mineral., 62,* 921–931.

Zachariasen, W. H. (1967) A general theory of X-ray diffraction in crystals. *Acta Crystallogr., 23,* 558–564.